AIP | Applied Physics Letters

Optically transparent glass micro-actuator fabricated by femtosecond laser exposure and chemical etching

Bo Lenssen and Yves Bellouard

Citation: Appl. Phys. Lett. **101**, 103503 (2012); doi: 10.1063/1.4750236
View online: http://dx.doi.org/10.1063/1.4750236
View Table of Contents: http://apl.aip.org/resource/1/APPLAB/v101/i10
Published by the American Institute of Physics.

Optically transparent glass micro-actuator fabricated by femtosecond laser exposure and chemical etching

Bo Lenssen and Yves Bellouard[a)]
Department of Mechanical Engineering, Eindhoven University of Technology, Eindhoven, The Netherlands

(Received 8 March 2012; accepted 20 August 2012; published online 5 September 2012)

Femtosecond laser manufacturing combined with chemical etching has recently emerged as a flexible platform for fabricating three-dimensional devices and integrated optical elements in glass substrates. Here, we demonstrate an optically transparent micro-actuator fabricated out of a single piece of fused silica. This work paves the road for further functional integration in glass substrate and optically transparent microsystems. © *2012 American Institute of Physics*. [http://dx.doi.org/10.1063/1.4750236]

Recent progresses in femtosecond laser processing of fused silica have opened up tremendous opportunities not only for integrated optics[1] but also—when combined with chemical etching[2]—for the fabrication of micro-channels and trenches.[3] Although counter-intuitive at first, femtosecond laser micromachined fused silica has excellent mechanical properties,[4] making possible the concept of all-in-glass opto-mechanical devices[5] that combines flexures and waveguides. Here, we demonstrate a monolithic glass micro-actuator, transparent over a large optical spectrum (from 400 nm to 1.6 μm), and fabricated using femtosecond laser processing.

The actuator, shown in Fig. 1 (left), performs an in-plane linear motion along one axis. It consists of two elements: a comb-array, formed by two intertwined sets of parallel beams and a flexure made of four leaf springs. Thanks to optically transparent electrodes deposited on the device; each set of parallel beams (Fig. 1 right) are put under different electrical potential and forms a capacitor.

One side of the comb-array is free to move while the opposite side is fixed. As a voltage is applied across the beams, a net force arises—due to asymmetrical gaps between cantilever beams, moving the mobile element along the Y-axis (see Fig. 1). The flexure, on which one side of the comb-array is attached, precisely guides the motion of the actuator and maintains the comb-array beams parallel to one another. The kinematics of this flexure is equivalent to two four-bar mechanisms mounted in series so that the off-axis motion of one of the four-bar mechanism exactly compensates the motion of the second one.[10] We recently demonstrated[4] that femtosecond laser processed silica flexures exhibit outstanding mechanical performances with breaking stress that can be well above 1.5 GPa.

Comb-array actuators and sensors are commonly used in silicon-based microsystems (see, for instance, Refs. 6–9). Here, we briefly describe its working principle. Actuation is achieved by the principle of variable capacitance. When a potential difference is applied between the two electrodes, an electrostatic force of attraction arises in a direction normal to the beams surfaces. In order to achieve a net force in one direction only, beams are distributed asymmetrically. The smallest and largest gaps between beams are noted d and g, respectively. As d is an order of magnitude smaller than g, the force acting towards the largest gap g is negligible. In a first approximation, the net normal force between the capacitor beams can be approximated by

$$F_{Tot} = N_A\left(\frac{\varepsilon_0 A V^2}{2d^2}\right), \tag{1}$$

where A is the surface between parallel plates, V is the applied voltage to the capacitors, ε_0 is the permittivity of air, d is the smallest gap between the two parallel plates, and N_A is the number of parallel actuators. The restoring force is provided by the elasticity of the flexure.

The linear stiffness for an applied force F_y along the y axis (i.e., along the motion direction) for a double compound flexure is given by

$$K_{F_y,u_y} = w\left(\frac{h}{L}\right)^3 E. \tag{2}$$

In mechanical equilibrium, the sum of all forces applied on the mobile element is zero, thus

$$\sum F = K_{F_y,u_y} u_y - F_{Tot} = K_{F_y,u_y}(d_0 - d) - N_A\left[\frac{\varepsilon_0 A V^2}{2d^2}\right] = 0, \tag{3}$$

where u_y is the displacement applied on the flexure and d_0, the initial gap. This equation is a third-order polynomial. The positive solutions of Eq. (3) are shown graphically in Fig. 2 for various voltages V. Out of the two possible positive mathematical solutions, only one leads to a stable mechanical equilibrium. Above a given voltage, so-called "pull-in voltage" (here 35 V in Fig. 2), there is no more positive solution and the system becomes unstable.

The positive solution of this polynomial (below the pull-in voltage) can be found analytically using the trigonometric version of Cardan's method for solving third order polynomial. It consists of expressing the polynomial in the form $x^3 + px + q = 0$ (where p and q are coefficients) to use a trigonometric identity $\{\cos(3\theta) = 4\cos^3\theta - 3\cos\theta\}$ to express the solutions in the form (for $p < 0$)

a)Author to whom correspondence should be addressed. Electronic mail: y.bellouard@tue.nl.

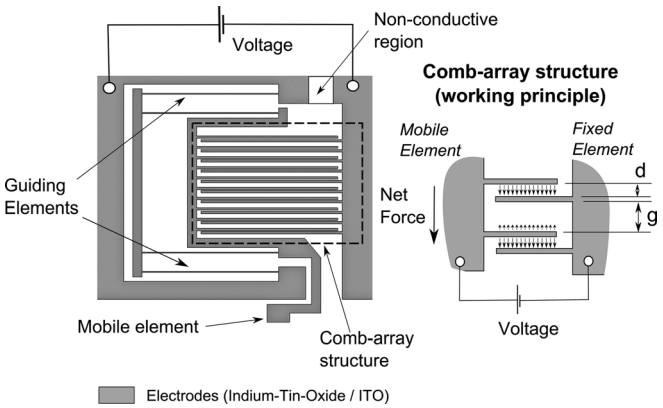

FIG. 1. Schematic of the glass actuator design. The design combines two elements. A comb-array that consists of a series of beams, parallel one to another and a flexure made of four leaf springs. The working principle of the variable capacitive actuator is illustrated on the right (for clarity, only forces viewed from the mobile element are shown). When a voltage is applied, the electrostatic force pulls the two parallel plates together. As one side of the mechanism is fixed, this electrostatic force results in a net force applied on the mobile element only. As such, comb-array actuators are mechanically unstable (i.e., a slight off-axis disturbance would collapse it). A mechanical guiding element that here consists of four leaf springs forming a double-compound linear guidance is used to keep the comb-array beams parallel to one another during actuation, preventing it from collapsing. A transparent conductive layer (indium-tin-oxide) is deposited everywhere on the material except for a small portion which remains uncovered and isolates electrically the two sides of the actuator.

$$\begin{cases} x_k = 2\sqrt{\frac{-p}{3}}\cos\left\{\frac{1}{3}\arccos\left(\frac{3q}{2p}\sqrt{\frac{-3}{p}}\right)+\frac{k\pi}{3}\right\} \text{ with } k=0,1,2 \\ p=-\frac{d_0^2}{3} \text{ and } q=-\frac{2}{27}d_0^3+\frac{\varepsilon_0 N_A A V^2}{2 K_{F_y,u_y}} \end{cases} . \tag{4}$$

The device is fabricated using a two-step process described in detail elsewhere.[3] The first step is to expose a fused silica substrate to low-energy pulses, well below the ablation threshold. During this operation, the material structure is locally modified, resulting in an accelerated HF etching rate in the laser exposed regions.

The exposure step is done with 380 fs-long pulses emitted at 1030 nm from a diode pumped Ytterbium-KGW crystal based femtosecond oscillator (t-Pulse 500 from Amplitude Systèmes). The oscillator emits pulses at a frequency of 9.4 MHz. An acousto-optic modulator (AOM) is used to reduce the repetition rate by chopping out pulses from the main pulse train. For fabricating this device, we used a repetition rate of 860 kHz. The laser beam is focused using a 20× objective (OFR-20X-1054) with a numerical aperture (NA) of 0.40. Using three linear positioning stages, the specimen is moved with an accuracy of 1 μm under the objective. The writing speed is 5 mm/s and the pulse energy is 215 nJ.

The second process step is a chemical etching step. The laser modified-substrate is immersed into a low-concentration HF bath (2.5%) for 18 h. In these conditions, the width after etching of a single laser exposed line profile is 22 μm. Considering the size of the laser affected zones (<2 μm), we estimate the etching time in the exposed region to be about 1 μm/min, while it slowed down to 1 μm/h in the bulk. Figure 3 shows the trench profile after etching. The etchant progresses simultaneously from top and bottom surfaces, gradually moving inside the material until the two etching front meet. The point across the section where the two etching fronts merged is found exactly in the middle, which indicates that despite the thickness of the substrates (>500 μm) and the increasing spherical aberrations associated with deeper laser-exposed patterns, the etching rate was rather homogeneous from top to bottom. Although the tapper here is quite small (less than 0.5°), it can be totally suppressed by modifying the laser pattern (see, for instance, Ref. 11) or using a KOH etchant that provides higher aspect ratio than HF as demonstrated in Ref. 12. For this device, the machining aspect ratio is 1:25.

Finally, a transparent electrode (indium-tin-oxide or ITO) is deposited on the micro actuator using RF-sputtering, down to the trenches, forming capacitors between plates. To prevent the ITO from covering the complete device, a simple

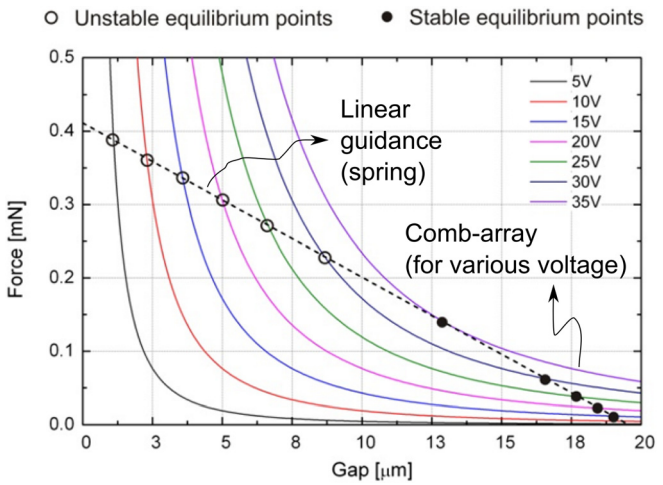

FIG. 2. Graphical representations of the actuators force/gap relation for various voltages (plain colored lines) and flexure mechanical characteristic (dashed line). The intersection points of the dashed line and plain curves are the positive solutions of Eq. (3). Among these positive solutions, only one set forms mechanically stable equilibrium points (shown here with a black dot).

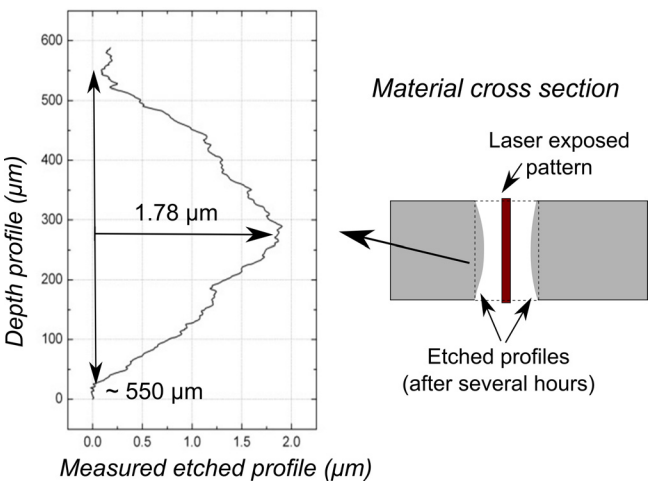

FIG. 3. Measured profile and schematic of a trench cross section after exposure of a single line pattern across the substrate thickness. The measurement is performed using a digital holographic microscope (Lyncée Tec, DHM 10020).

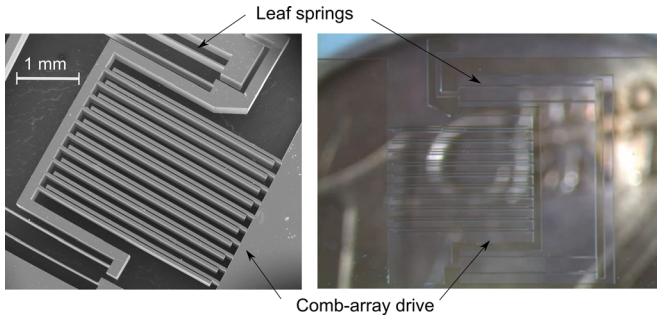

FIG. 4. Scanning electron microscope image (left) of the micro actuator. The comb-array electrode and part of the leads springs are shown. The surface of the substrate has a 100 nm-conductive ITO layer. Video capture (right) of the micro actuator at approximately 1 Hz and an applied voltage of 35 V. A 1-cent Euro-coin is visible in the background. The leaf springs are 3 mm long, 20 μm in height, and 0.5 mm thick (enhanced online) [URL: http://dx.doi.org/10.1063/1.4750236.1].

protective tape used as a hard-mask is manually placed before sputtering on the etched substrate (see Fig. 1 left, "uncoated region"). This tape is later removed, leaving a part of the device uncoated and used as insulator for the two electrodes.

A scanning electron microscope (SEM) image of the device and a video-snapshot of the actuator moving are shown in Fig. 4. In the related video, to illustrate the optically transparent properties of the actuator, the microscope focal plane is moved across the actuator.

We use a triangulation position sensor (Keyence, LK-G10) to measure the displacement of the actuator upon application of a voltage across the electrodes. The experimental results are shown in Fig. 5 and compared to the actuator model proposed earlier [using Eq. (4), adjusted to our experimental conditions]. We observe a good agreement between the actuator model and the effective measurements.

The dynamic performances of the actuator were measured using a laser vibrometer (Polytec PI OFV-552). We found the main resonant peak at 460 Hz and the second resonant mode (corresponding to the vibration of the intermediate body) around 1960 Hz. The results are shown in Figure 6 and compared to a classical model (red curve) consisting of two masses connected with springs (using the

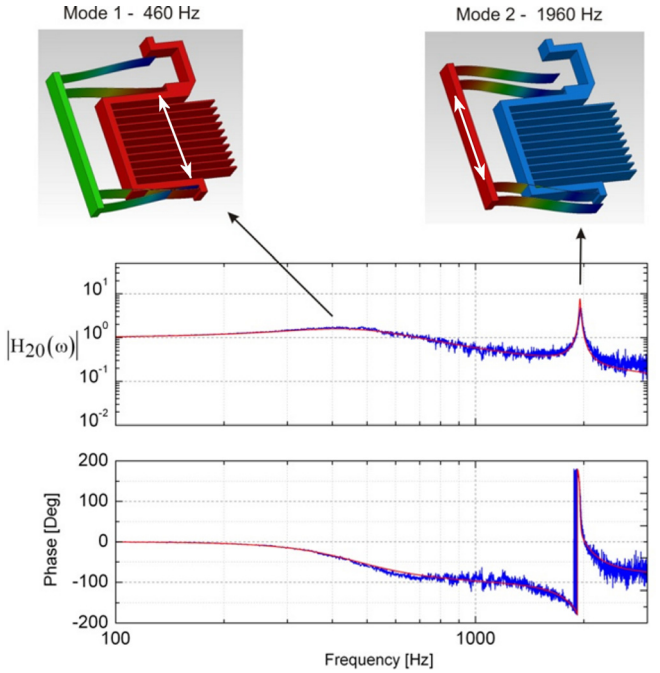

FIG. 6. Dynamic response of the transparent capacitive actuator. The red and blue curves correspond, respectively, to a simulation and the actual measurement. The two first vibrations modes are highlighted with two finite-element modeling shown above.

stiffness matrix of Eq. (3)) and dampers. The first mode is highly damped due to a squeezed-film effect due to the air present in between capacitor plates. This effect is captured in the simulation by a simple damper that connects the actuator end-effector to the actuator frame. The second mode shows a high resonance due to the internal mobility of the double-compound mechanism (i.e., the intermediate body can still move if the end-effector is kept still). This second vibration mode can be suppressed by removing this internal mobility which would require coupling the end-effector to the intermediate body through a master-slave mechanism.

In conclusion, we have demonstrated an optically transparent micro-actuator manufactured using femtosecond laser and chemical etching. This work comes as a sequel of a

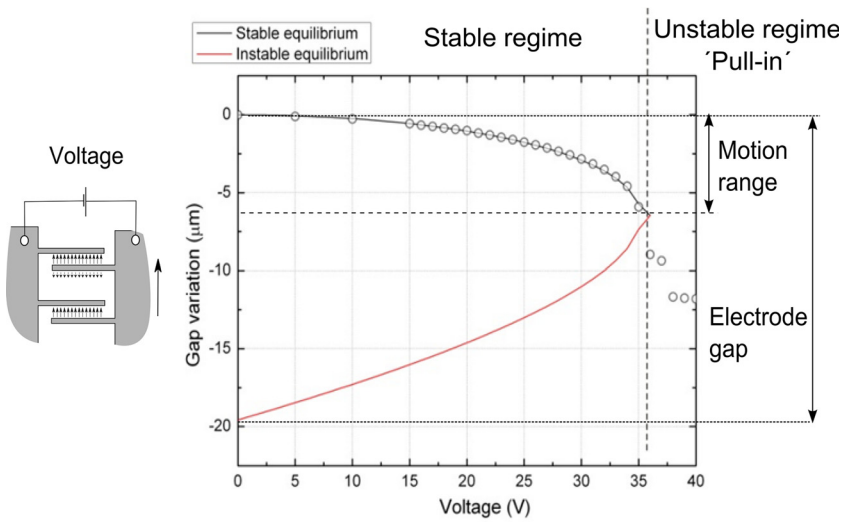

FIG. 5. Positive solutions (see Eq. (6)) of Eq. (5) as a function of the applied voltage and actual measurement points (circles). The black curve is the mathematical solution corresponding to a stable equilibrium while the red one forms unstable points. Above a given voltage—the so-called "pull-in" voltage (here around 35 V), the actuators enters an unstable regime. Errors bars for the measurements are estimated to be $\pm$ 0.2 V and $\pm$ 0.1 μm.

demonstration of a monolithic displacement sensor that integrated waveguides and mechanical element[5] by demonstrating that femtosecond laser manufacturing can also be used to implement active mechanical function in a functional silica substrate.

The actuator transparency is only limited by the ITO layer (the electrodes) that has a transmittance varying between 80% and 90% from 400 nm to 1.6 μm depending on sputtering conditions and post-annealing process.

Transparent actuator can be used in various optical applications such as adaptive optics and microscopy. Glass actuator can also form the moving basis for Michelson interferometer or alike such as Fourier-transform interferometer in which the optical information travels through the glass structure. Thanks to the broad transparency spectral range of fused silica; transparent actuators can be used for creating tunable resonant cavities in the visible spectrum. Last but not least, such actuator can be combined with a variety of integrated optical elements (like waveguides,[1,13] polarization converter devices,[14] bulk-laser fabricated micro-optical components,[15] direct-write Fresnel lenses,[16,17] and bulk Bragg-gratings[18]) themselves manufactured with the *same* femtosecond laser, opening interesting opportunities for all-optical devices and transparent MEMS made-out of a single piece of silica.

This work is supported by the Femtoprint project (http://www.femtoprint.eu/) of the 7th Framework programme of the European Commission as part of the NMP/Factory of the Future initiative. The author acknowledges the help of Erik Homburg for setting-up the Keyence sensor.

[1]K. M. Davis, K. Miura, N. Sugimoto, and K. Hirao, Opt. Lett. **21**, 1729–1731 (1996).
[2]A. Marcinkevičius, S. Juodkazis, M. Watanabe, M. Miwa, S. Matsuo, H. Misawa, and J. Nishii, Opt. Lett. **26**, 277–279 (2001).
[3]Y. Bellouard, A. Said, M. Dugan, and P. Bado, Opt. Express **12**, 2120–2129 (2004).
[4]Y. Bellouard, Opt. Mater. Express **1**, 816–831 (2011).
[5]Y. Bellouard, A. Said, and P. Bado, Opt. Express **13**, 6635–6644 (2005).
[6]R. Legtenberg, A. W. Groeneveld, and M. Elwenspoek, J. Micromech. Microeng. **6**, 320–329 (1996).
[7]C. Marxer and N. F. de Rooij, J. Lightwave Technol. **17**, 2–6 (1999).
[8]M. Tormen, Y.-A. Peter, P. Niedermann, A. Hoogerwerf, and R. Stanley, J. Opt. A, Pure Appl. Opt. **8**, S337–S340 (2006).
[9]S. Muntwyler, F. Beyeler, and B. J. Nelson, J. Micromech. Microeng. **20**, 025011 (2010).
[10]R. V. Jones, J. Sci. Instrum. **28**, 38–41 (1951).
[11]K. C. Vishnubhatla, N. Bellini, R. Ramponi, G. Cerullo, and R. Osellame, Opt. Express **17**, 8685–8695 (2009).
[12]S. Kiyama, S. Matsuo, S. Hashimoto, and Y. Morihira, J. Phys. Chem. C **113**, 11560–11566 (2009).
[13]S. Nolte, M. Will, J. Burghoff, and A. Tuennermann, Appl. Phys. A: Mater. Sci. Process. **77**, 109–111 (2003).
[14]M. Beresna, M. Gecevicius, P. G. Kazansky, and T. Gertus, Appl. Phys. Lett. **98**, 201101 (2011).
[15]Y. Cheng, K. Sugioka, K. Midorikawa, M. Masuda, K. Toyoda, M. Kawachi, and K. Shihoyama, Opt. Lett. **28**, 1144–1146 (2003).
[16]E. Bricchi, J. D. Mills, P. G. Kazansky, B. G. Klappauf, and J. J. Baumberg, Opt. Lett. **27**, 2200–2202 (2002).
[17]P. Srisungsitthisunti, O. K. Ersoy, and X. Xu, J. Opt. Soc. Am. B **24**, 2090–2096 (2007).
[18]G. D. Marshall, M. Ams, and M. J. Withford, Opt. Lett. **31**, 2690–2691 (2006).